

Effect of prestrain and strain path on Retained Austenite transformation and eventual fracture behavior of Q&P steels

Sriram Sadagopan^{1*}, Brian Lin¹, Narayan Pottore¹, Su Liu¹, and Hong Zhu¹

¹ArcelorMittal USA Research LLC, 3001 E. Columbus Drive, E. Chicago, IN 46312, USA

Abstract. Post-forming fracture behavior of Quenched & Partitioned (Q&P) steel grades can be compromised because of reduction of available Retained Austenite (RA) and formation of fresh martensite during stamping. A study was undertaken to characterize the post-forming fracture behavior of two Q&P steel grades of tensile strength 980MPa and 1180MPa. Using the Marciniak test, samples were formed to different strain levels under plane strain and balanced biaxial conditions. Following forming, samples were extracted to determine the fracture strain using the VDA238-100 bend test with Digital Image Correlation (DIC). In both steels, it was found that while the post-forming fracture strain had a strong dependence on the remaining RA after pre-straining, the strain path had a lower influence.

Keywords: Q&P; Prestrain; Fracture; Partitioning

1 Introduction

Cold stamped Advanced High Strength Steels (AHSS) have been successfully developed and utilized in automotive body structures in the last two decades. The newest third-generation AHSS grades, also called Quenched & Partitioned (Q&P) steels [1, 2], offer the best combination of strength and ductility. This results from the presence of retained austenite (RA) in the microstructure, which enhances the work hardenability and formability through the transformation of austenite to martensite enabling cold stamping of complex parts. The change in constituent microstructure during stamping also impacts various property attributes of the steel. Numerous investigations have been conducted over the years to understand the factors that influence the transformation of RA to martensite during deformation and resulting impact on steel properties [3-17]. Full comprehension of the microstructural transformation and mechanical behavior of these steels during and post deformation is essential for optimizing press formability and efficient end-use implementation of the stamped component in automotive structures

The effect of microstructural features in Q&P steels especially the effect of near neighbourhood phases, their morphology and strength, and effect on crack propagation has been studied by multiple investigators [3-5]. The role of fresh martensite on the stability of RA has been specifically investigated as well [6]. The impact of strain path on RA transformation behavior has also been explored in some studies [7-8]. The contribution to increased formability by optimizing the martensitic component within the microstructure has also been researched [9].

Investigators have also characterized the impact of RA transformation to martensite on the evolution of damage [10], fracture [11], fatigue [12], toughness [13,14], and susceptibility to hydrogen embrittlement [15,16]. Since as-stamped components in the vehicle structure are also subjected to paint baking, one investigation has characterized the impact toughness properties of a Q&P steel after the strained and baked state [17].

The previous characterization studies on Q&P steels have mostly focused on transformation kinetics of RA caused by uniaxial deformation, not forming conditions. Furthermore, industrial stamping will typically include different strain paths, which may result in differences in austenite to martensite phase transformation. Additionally, the residual ductility in the material after prestraining is also an important attribute to consider to holistically evaluate material performance in actual applications. This paper adds to our understanding of RA containing steels with a combined focus on the extent of strain and strain path dependency of RA transformation and the post-forming fracture ductility of two specific Q&P steels.

2 Methods and procedures

2.1 Materials

Two of ArcelorMittal's Hot Dipped Galvanized (GI) coated Q&P steel grades: Fortiform®980 and Fortiform®1180 were selected for the study. Table 1 shows the summary mechanical properties of the two steels with Fig. 1 showing the work hardening behavior.

* Corresponding author: sriram.sadagopan@arcelormittal.com

Fig. 2 shows the microstructure of the two steels obtained using a Scanning Electron Microscope (SEM).

Table 1. Mechanical Properties of the steels used in the study

Steels (GI)	YS (MPa)	TS (MPa)	TE (%)	Min. R/t
Fortiform®980	630	1019	21	<1.0
Fortiform®1180	1005	1219	17	<1.0

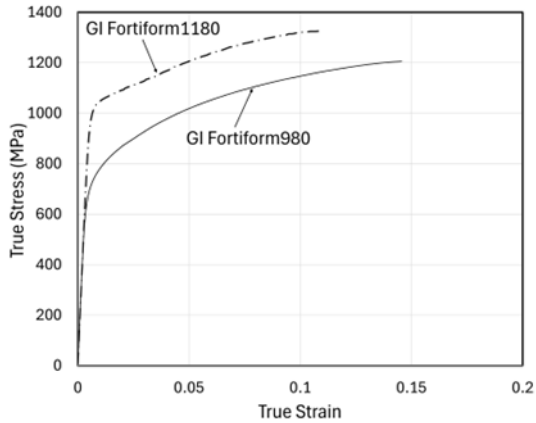


Fig. 1. Work hardening behavior of the steels in the study

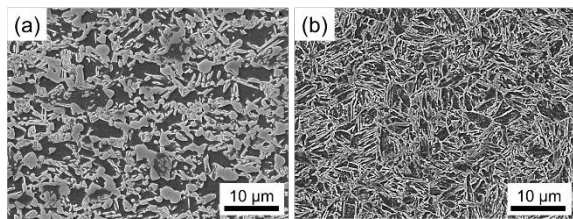


Fig. 2. Microstructures of (a) GI Fortiform®980 and (b) GI Fortiform®1180

As seen in Fig. 1, the hardening behavior in the initial stages of work hardening is significantly different between the grades. This can be attributed to the differences in microstructures, where Fortiform®980 has considerably more ferrite than Fortiform®1180. This results in a higher property gradient in the microstructure for the GI Fortiform®980, resulting in the ferrite accommodating much of the deformation in the early stages of tensile loading, leading to a higher work hardening rate.

Additionally, X-ray diffraction (XRD) measurements were performed using a conventional PANalytical X’Pert Pro MPD [MultiPurpose Diffractometer] X-ray diffractometer with a Co-K α sealed-tube source operated at 30 kV and 50 mA to produce a wavelength of 1.79 Å. Samples were prepared by surface grinding and removing a quarter thickness of the starting material. The Bragg–Brentano focusing geometry was employed to collect diffraction patterns over the 2 θ range from 55 to 130 degrees with a step size of 0.05 degrees. The commercially available X-pert HighScore Plus software was used to analyze the Ferrite 200, 211, and 220, and the austenite 200, 220, 311 peaks. The average RA volume fraction was calculated from all available pairs of lines as described by Cullity [18]. Figs. 3 and 4 show the XRD scans for

GI Fortiform®980 and GI Fortiform®1180 respectively.

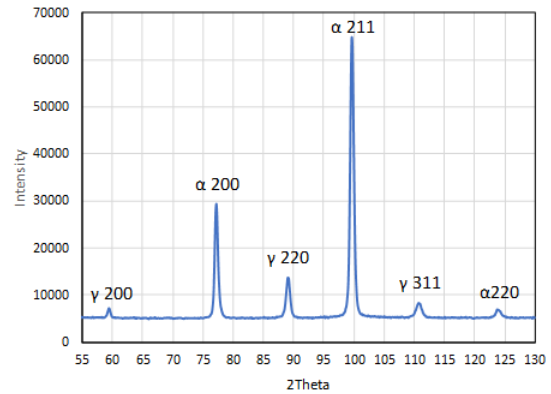


Fig. 3. XRD scans of GI Fortiform®980

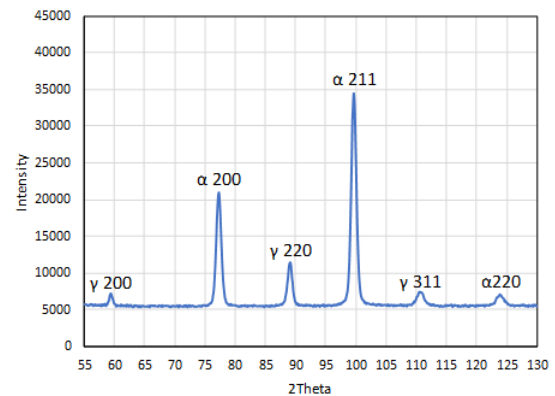


Fig. 4. XRD scans of GI Fortiform®1180

The phase fractions of constituents in the two grades determined using XRD are shown in Table 2. Of significance is the similarity in RA content between the two grades but a sharp reduction in ferrite content and increase in bainite and tempered martensite content in Fortiform®1180. The fresh martensite content is also similar in the two steels in the as manufactured state.

Table 2. Summarized microstructural details of the two grades (F: Ferrite, B: Bainite, TM: Tempered Martensite, RA: Retained Austenite, FM: Fresh martensite)

	Fortiform®980	Fortiform®1180
% F	40	2
% B + TM	43	81
% RA	14	14
% FM	3	3

2.2 Experiments

The experimental procedure consisted of:

- **Prestraining samples:** Samples were prestrained using a cylindrical punch and drawbead combination, also called the Marciniak tooling [19] shown in Fig. 5, which is typically used for determination of in-plane forming limits. Two sample geometries were used to form domes to different heights to generate several strain magnitudes before failure by incipient necking for the two strain paths.



Fig. 5. Marcink tooling and prestrained samples for biaxial and plane strain conditions

- **Post forming RA Determination & Bend Fracture Strain:** Coupons were extracted from the formed parts for XRD measurements as described earlier to determine the RA volume fraction and for fracture strain determination using the VDA238-100 bend test [20]. Fig. 6 shows the schematic of the test. The sheet is bent with the axis along the Rolling Direction and the load deflection curve monitored with the drop in load corresponding to material failure. Additionally, Digital Image Correlation (DIC) was used to determine the major strain and minor strain at the tension side of the bent sheet to determine the failure strain. Fig. 7 shows the load deflection curve from the test and the DIC images of major and minor strain at the point of maximum load. The test was automatically stopped when the drop in load from the maximum point reached 60N.

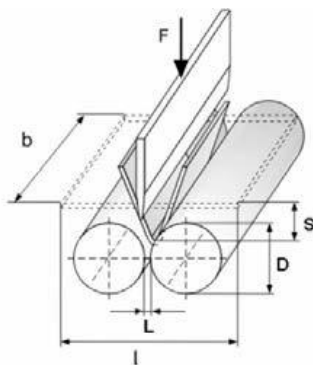


Fig. 6. Schematic of VDA bend test [20]

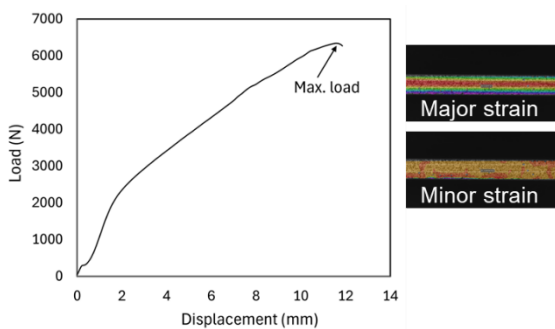


Fig. 7. Load deflection curve from the VDA bend test [20] coupled with strain measurements using DIC showing the major and minor strain at the tension side of the bent sheet.

Analysis of major and minor strain evolution indicated negligible minor strain (plane strain condition) throughout the test duration. The major strain at the point of fracture in the test is used as a measure of post-forming fracture strain.

3 Results and discussion

Figs. 8 and 9 show the RA volume fraction as a function of prestrain for the two steel grades, for three different strain paths, as determined by XRD. As expected, the magnitude of achievable prestrain in the biaxial strain path is considerably higher than the uniaxial or plane strain paths.

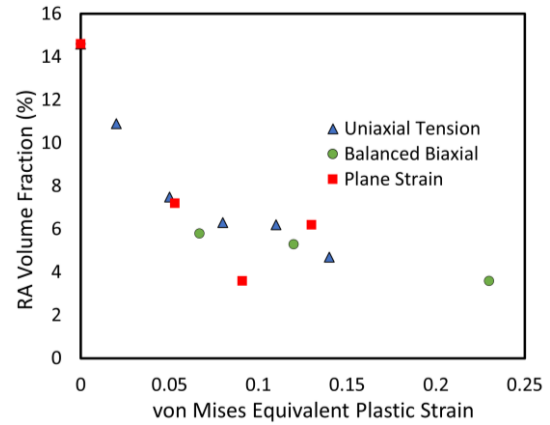


Fig. 8. RA volume fraction after in-plane prestraining for GI Fortiform®980

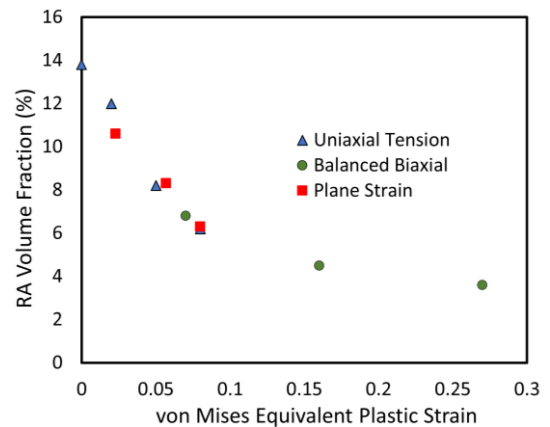


Fig. 9. RA volume fraction after in-plane prestraining for GI Fortiform®1180

As seen in Figs. 8 and 9, per expectation, the RA volume fraction decreases with increasing magnitude of prestrain, expressed here as the von Mises equivalent plastic strain. Additionally, the effect of strain path was observed to be secondary when compared to the magnitude of prestrain.

Fig. 10 shows the post-forming fracture strain determined by DIC-assisted VDA bend test, plotted against the residual RA volume fraction after prestrain.

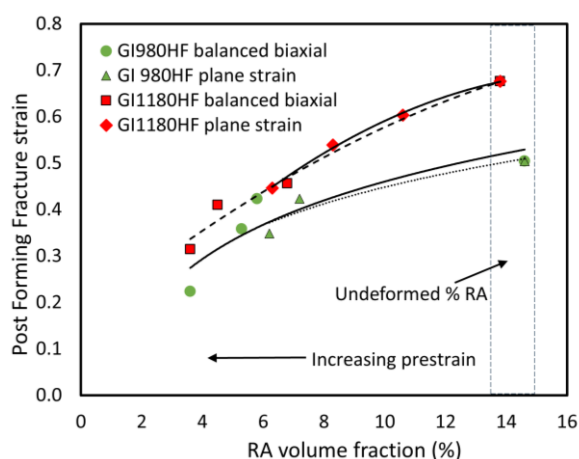


Fig. 10. Fracture strain dependence on RA volume fraction resulting from prestraining

The dotted vertical lines in the figure shows the range of %RA for the two grades in the undeformed condition. The reduction in post-forming fracture strain is as expected and correlates well with the decreasing RA volume fraction with increasing prestrain and shows a low dependence on strain path. However, upon comparing this behavior in the two steels, even with a similar change in RA with prestrain, the reduction in the fracture strain in Fortiform®1180, is significantly higher than that in Fortiform®980. This could be attributed to two factors: (a) higher initial fracture strain in the Fortiform®1180 originating from its microstructural characteristics, especially its refined nature and near equivalent strength of its principal constituent phases - bainite, tempered martensite and retained austenite [21], and (b) difference in the strain partitioning behavior between the two steels. Unlike Fortiform®1180 which is largely devoid of ferrite, during the initial straining in Fortiform®980, it is ferrite that undergoes significant straining leaving RA largely untransformed. Hence, the slope of the curve showing the reduction in fracture strain with retained austenite content is less steep initially. When the ferrite has undergone a high level of strain, its constituent strength begins to approach that of bainite, tempered martensite and retained austenite. Straining beyond this point results in a more even loading pattern amongst the constituent phases [3]. The increase in fresh martensite due to the transformation of RA and its interaction with a predominantly bainitic/tempered martensitic structure results in crack initiation and propagation as deformation continues. This phenomenon is being investigated further.

4 Conclusions

Post forming fracture behavior of coated Q&P steels was evaluated using a combination of in-plane stretching and DIC-assisted VDA bend testing. Results show a decrease in post-forming RA volume and fracture strain with increasing prestrain, with a weaker dependence on strain path. Furthermore, the extent of fracture strain reduction seems to be higher in Fortiform®1180. Further work needs to be conducted to fully understand this behavior.

References

1. J. G. Speer, D. K. Matlock, B. C. DeCooman, and J. G. Schroth, *Acta Mat.*, **51**, 16 (2003).
2. J. G. Speer, A. M. Streicher, D. K. Matlock, F. Rizzo, and G. Krauss, *Quenching and Partitioning: A Fundamentally New Process to Generate High Strength TRIP Sheet Microstructures*, in *Austenite Formation and Decomposition*, The Iron & Steel Society and TMS (2003).
3. J. Kang, N. S. Pottore, H. Zhu and C. C. Tasan, *Acta Mat.*, **254** (2023).
4. H. S. Zhao, W. Li, X. Zhu, X. H. Lu, L. Wang, S. Zhou and X. J. Jin, *Mat. Sci. and Engg. A*, **649**, 18 (2016).
5. D. Knijf, C. Fojer, L. Kestens and R. Petrov, *Mat. Sci. and Engg. A*, **638**, 219 (2015).
6. D. Knijf, R. Petrov, C. Fojer and L. Kestens, *Mat. Sci. and Engg. A*, **615**, 107 (2014).
7. J. Cramer, D. Adams, M. P. Miles, D. T. Fullwood, E. R. Homer, T. Brown, R. K. Mishra and A. K. Sachdev, *Mat. Sci. and Engg. A*, **734**, 192 (2018).
8. P. Gibbs, D. Adams, D. T. Fullwood, E. R. Homer, A. K. Sachdev and M. P. Miles, *J. Manuf. Mat. Process*, **9**, 75 (2025).
9. K. O. Findley, J. Hidalgo, R. M. Huizenga and M. J. Santofimia, *Mat. and Design*, **117**, 248 (2017).
10. C. Pelligra, J. Samei, B. S. Amirkhiz, L. G. Hector and D. S. Wilkinson, *Mat. Sci. and Engg. A* **895**, 146181 (2024).
11. I. de. Diego-Calderon, I. Sabirov, J. M., Molina-Aldareguia, C. Fojer, R. Thiessen, and R. H. Petrov, *Mat. Sci. and Engg. A* **657**, 136 (2016).
12. I. de. Diego-Calderon, P. Rodriguez-Calvillo, A. Lara, J. M. Molina-Aldareguia, R. H. Petrov, D. Knijf and I. Sabirov, *Mat. Sci. and Engg. A* **641**, 215 (2015).
13. R. Wu, W. Li, S. Zhou, Y. Zhong, L. Wang and X. Jin, *Met. and Mater. Trans. A*, **45A**, 1892 (2014).
14. K. Yang, Y. Li, Z. Hong, S. Du, T. Ma, S. Liu and X. Jin, *Mat. Sci. and Engg. A*, **820**, 141517 (2021).
15. X. Zhu, K. Zhang, W. Li and X. Jin, *Mat. Sci. and Engg. A* **658**, 400 (2016).
16. K. J. Kim, S. Y. Song, G. Lee, H-J. Kim, H. Y. Um, J-S. Hyun, S-P Jung, K. Ryou, P-P Choi, A. Zargarani, M-G Lee and S. S. Sohn, *Mat. Sci. and Engg. A* **913**, 147008 (2024).
17. A. D. Hodges, S. Tedesco, L. Golem and G. Huang, SAE Technical Paper 21021-01-0266 (2021).
18. B.D. Cullity, *Elements of X-ray Diffraction*, 2nd Edition, (1978).
19. Z. Marciniak and K. Kuczynski, *Int. J. Mech. Sci.* **9**, 609 (1967).
20. Plate Bending Test for Metallic Materials VDA 238-100.

21. K-S Kim, C. Okuyucu, N.S. Pottore, H. Zhu and C.C. Tasan, J. Mat. Proc. Tech. (to be published)